Towards nanometric resolution in multilayer depth profiling: a comparative study of RBS, SIMS, XPS and GDOES

Ramón Escobar Galindo · Raul Gago · David Duday · Carlos Palacio

Abstract An increasing amount of effort is currently being directed towards the development of new functionalized nanostructured materials (i.e., multilayers and nanocomposites). Using an appropriate combination of composition and microstructure, it is possible to optimize and tailor the final properties of the material to its final application. The analytical characterization of these new complex nanostructures requires high-resolution analytical techniques that are able to provide information about surface and depth composition at the nanometric level. In this work, we comparatively review the state of the art in four different depth-profiling characterization techniques: Rutherford backscattering spectroscopy (RBS), secondary ion mass spectrometry (SIMS), X-ray photoelectron spectroscopy (XPS) and glow discharge optical emission spectroscopy (GDOES). In addition, we predict future trends in these techniques regarding improvements in their depth resolutions. Subnanometric resolution can now be achieved in RBS using magnetic spectrometry systems. In SIMS, the use of rotating sample holders and oxygen flooding during analysis as well as the optimization of floating low-energy ion guns to lower the impact energy of the primary ions improves the depth resolution of the technique. Angle-resolved XPS provides a very powerful and nondestructive technique for obtaining depth profiling and chemical information within the range of a few monolayers. Finally, the application of mathematical tools (deconvolution algorithms and a depth-profiling model), pulsed sources and surface plasma cleaning procedures is expected to greatly improve GDOES depth resolution.

Keywords Depth profiling · XPS · SIMS · GDOES · RBS · Multilayer · High resolution

R. Escobar Galindo
Centro de Micro-Análisis de Materiales,
Universidad Autónoma de Madrid,
28049 Madrid, Spain

R. Escobar Galindo (✉) · R. Gago
Instituto de Ciencia de Materiales de Madrid,
Consejo Superior de Investigaciones Científicas,
28049 Madrid, Spain
e-mail: rescobar@icmm.csic.es

D. Duday
Département de Science et Analyse des Matériaux,
Centre de Recherche Public Gabriel Lippmann,
41 rue du Brill,
Belvaux 4422, Luxembourg

C. Palacio
Departamento de Física Aplicada,
Universidad Autónoma de Madrid,
Cantoblanco 28049 Madrid, Spain

Introduction

The current road to miniaturization (i.e., sub-32 nm technologies) demands novel or advanced analytical techniques with extremely high depth resolutions that are capable of characterizing sample features on the nanoscale [1–3]. In particular, ultrathin layers and multilayer systems are gaining increasing interest because they can exhibit novel structural, physical and chemical properties that differ from those of the corresponding bulk materials. With the decreasing thicknesses of such layers, film characterization with depth resolutions at the scale of a few interatomic distances must be achieved. For a single interface between two layers A and B, the most common definition of the depth resolution as recommended by IUPAC and ASTM E-42 is Δz, which corresponds to the interval of the depth

coordinate z at an interface over which there is a 84% to 16% change in intensity [3].

Nowadays, the chemical analysis of these very thin films is carried out using either destructive or nondestructive methods. Actually, for thin films above 10 nm in thickness, the method most frequently applied to obtain the concentration depth profile (CDP)—that is, the composition of the thin film as a function of depth—is ion sputtering in combination with any of the well-known surface analysis techniques [4, 5]. Among these, X-ray photoelectron spectroscopy (XPS) [6, 7], secondary ion mass spectroscopy (SIMS) [8, 9], and, more recently, glow-discharge optical emission spectroscopy (GDOES) [10, 11] are becoming the most popular. In addition, Rutherford backscattering spectroscopy (RBS) is a nondestructive technique that is commonly employed for in-depth compositional analysis [12, 13]. The method that should be used depends specifically on the actual analytical problem to be solved, although the general trend is towards the simultaneous use of several techniques due to the complementary information provided. The principal multilayer systems (i.e., nitride, oxide, metal, etc.) have been extensively studied by a combined analyses, such as XPS-RBS [14–16], RBS-GDOES [17, 18], GDOES-SIMS [19, 20], SIMS-RBS [21, 22], XPS-GDOES [23], XPS-SIMS [24, 25], XPS-RBS-GDOES [26] or RBS-SIMS-GDOES [27].

In this paper we will review the current status of each of these four characterization techniques, as well as the most recent developments regarding improvements in the depth resolutions of these techniques. Relevant examples of their application to nanometer-scale multilayer analysis will be presented.

X-ray photoelectron spectroscopy (XPS)

Among the instrumental techniques used for the chemical analysis of solids, X-ray photoelectron spectroscopy (XPS) is one of the most appropriate for examining surfaces. It is based on Einstein's quantum interpretation of the photoelectric effect. This interpretation assumes that the energy of the emitted photoelectrons can be calculated as the difference between the incident photon energy and the binding energy (BE) of the electrons in the atoms of the sample. The modern XPS technique was originated by Siegbahn and coworkers at Uppsala University in Sweden in the mid-1950s. They developed a high-resolution spectrometer for determining the binding energies of the atomic shells of the less tightly bound orbitals. As a result of this program it was discovered that the BEs of the core electrons were dependent on the chemical environment; that is, the chemical shifts in XPS reflect changes in chemical bonding or oxidation state and can therefore be used to follow such changes on surfaces. XPS is sensitive (0.01 monolayers of most materials produce a detectable signal), quantitative, and signals can be measured for all elements except H and He. Strictly speaking, XPS is a surface technique, but it can also be used to analyze a layer of adsorbed material in order to see both the surface and the adsorbate, since only the electrons created in a zone characterized by a depth $\lambda\cos\theta$ (called the escape depth) from the surface escape to contribute to the XPS spectrum. Here λ is the attenuation length of the emitted photoelectron and θ is the angle of emission with respect to the surface normal. Values of λ lie in the range 0.5−2.5 nm, and this phenomenon makes XPS a surface-sensitive technique, as stated before.

Nowadays, when employed for depth-profiling analysis, XPS is most frequently used in combination with ion sputtering [28, 29]. An example of depth profiling with XPS is depicted in Fig. 1. The ultimate depth resolution depends on instrumental factors, the induced surface roughness, atomic mixing, enhanced induced diffusion and the information depth of the surface analysis technique used. However, applying some refinements can lead to reliable results, with depth resolutions as good as 1–2 nm [30–32]. Experimental CDPs are usually extracted from the intensity $I_i(t)$ that is characteristic of a sample component i as a function of the erosion time t. However, the desired result is the concentration $c_i(z)$ of each component as a function of the depth z. The problem is then the quantification of the experimental information to get the desired information. This quantitative evaluation of measured profiles involves the calibration of the thickness scale (that is, the conversion of the sputtering time into the sputtered depth) and the calibration of the concentration scale (that is, the conversion of the elemental signal intensity into the elemental concentration, and the correction/deconvolution of the effects that modify the depth resolution). The procedure used to perform the quantitative analysis is shown schematically in Fig. 2.

In most cases, the time → depth and intensity → concentration relations are practically linear and can easily be obtained from appropriate sputtering rates and elemental sensitivity factors, respectively [30, 31]. Effects that modify the depth resolution can be corrected for using the so-called resolution function $g(z'-z)$ along with Eq. 1 (below) in order to obtain the real concentration $c_i(z)$ using the appropriate deconvolution procedures [33, 34]:

$$c_i'(z') = \int_{-\infty}^{\infty} c_i(z)g(z'-z)dz \tag{1}$$

The resolution function can be modeled either experimentally or via theoretical models that take into account all of the abovementioned factors that modify the depth resolution. In fact, for the information depth of the surface

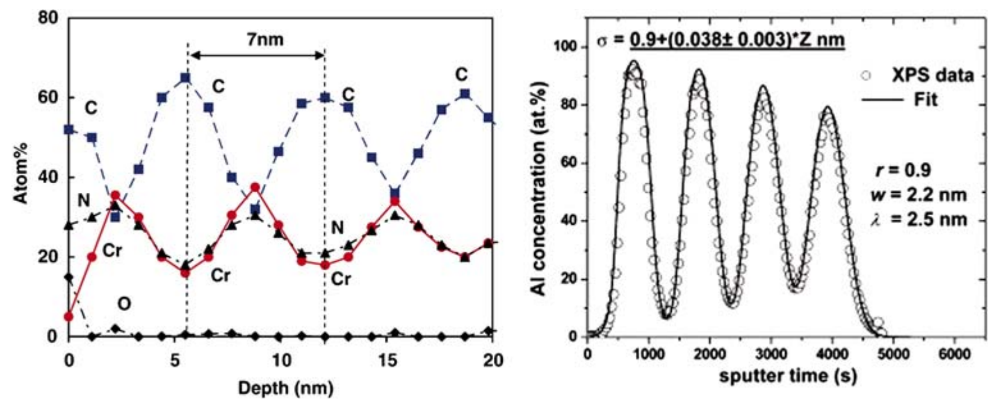

Fig. 1 XPS concentration–depth profiling data from a (*left*) Cr(N)/C(DLC) nano-multilayered coating (taken from [28] and reproduced with the permission of Elsevier) and (*right*) a 15 nm Si/15 nm Al multilayered system (taken from [29] and reproduced with the permission of Elsevier)

analysis technique used, the resolution function is properly represented by Eq. 2:

$$g(z-z') = \exp\left(-\frac{z-z'}{\lambda_i \cos\theta}\right) \tag{2}$$

where $\lambda_i\cos\theta$ is the attenuation length of the emitted photoelectrons, and θ is the take-off angle with respect to the surface normal [33].

For thin films with thicknesses below 10 nm, the changes that occur during ion bombardment before a steady state is established during the sputtering process make this approach completely inaccurate, and alternative methods must be used. Such methods, for example angle-resolved X-ray photoelectron spectroscopy (ARXPS), are nondestructive [32, 35, 36]. Since chemical information is very rapidly destroyed by depth-profiling methods that involve sputtering, angle-resolved methods are also advantageous for preserving chemical state information. Figure 3 shows a schematic diagram of the ARXPS experimental set-up. In this figure, λ stands for the attenuation length of the emitted photoelectrons. If spectra are recorded at different emission angles θ, the photoelectron escape depth, $\lambda\cos\theta$, can be varied in such a way that the depth probed is varied, so the set of angular measurements will contain information on the CDP of each species. The intensity of the emitted photoelectrons corresponding to a particular XPS band for a specific element is given by Eq. 3:

$$I_i(\theta) = \frac{I_i^0}{\lambda_i \cos\theta} \int_0^\infty c_i(x) \exp\left(\frac{-x}{\lambda_i \cos\theta}\right) dx \tag{3}$$

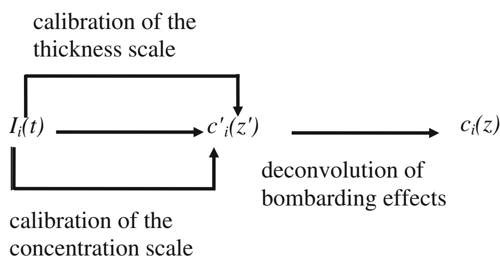

Fig. 2 Scheme of the depth-profile quantification procedure

where $c_i(x)$ is the concentration of element i at a depth x, assumed to be uniform at the surface, λ_i is the attenuation length of the photoelectrons from this element, θ is the take-off angle with respect to the surface normal, and I_i^0 is a constant that depends on instrumental factors, angular asymmetry and photoionization cross-section. Equation 3 is an integral equation of the first kind and represents a prototype for ill-posed problems [35]. Two different approaches have been used to extract the concentration depth profiles, $c(x)$: simple parametric models that make some assumption about the form of the depth profile (see the bottom panel of Fig. 3), and general algorithms that use regularization in addition to singular value decomposition (SVD) techniques [35] without any prior hypothesis for the shape of the concentration depth profile. In general, these methods display common limitations imposed by the low

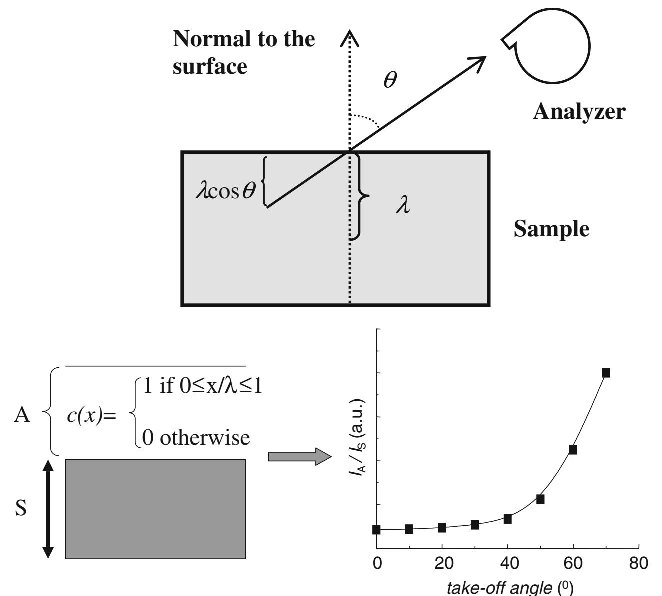

Fig. 3 *Top*: schematic diagram of the ARXPS experimental set-up. *Bottom*: schematic diagram of a step-like depth profile of a pure substrate S, covered by a layer A, of thickness $d = \lambda$ and constant composition. The simulated intensity ratio I_a/I_s as a function of the take-off angle is also shown (*right-hand side*). Taken from [35] and reproduced with the permission of Elsevier

information content of ARXPS measurements, with the depth resolution Δz limited to about 0.8z [32]. Although this is a poorer fractional depth resolution than sputter depth profiling allows in the depth range of ~10–500 nm, it is better than the sputter depth profiling in the near-surface (0–5 nm) region accessible to ARXPS. Anyway, the worst value for the depth resolution in this thickness interval is about 4 nm, as can be observed in the left-hand panel of Fig. 4. This figure shows the depth profiles calculated using the experimental data collected for an ultrathin layer prepared by the underpotential deposition (upd) of silver on polycrystalline platinum using the inversion procedure described above [35]. The regularization algorithm produces a reasonable estimate for the concentration depth profile where two layers can be observed: a surface carbon layer ~1.6 nm thick, followed by a complex layer containing S, O, and Ag with a thickness of ~1 nm. Figure 4 (right-hand panel) shows ARXPS results for a naturally oxidized Al layer [36]. According to the results shown in Fig. 3, an increase in the signal intensity (or, equivalently, the concentration) with increasing take-off angle indicates that the corresponding species is nearer to the surface than species that display the opposite behavior. Therefore, ARXPS of Fig. 4 (right-hand panel) indicates that C contamination covers the naturally oxidized Al layer [36]. It is important to point out that the depth resolution in ARXPS is limited by the signal-to-noise ratio, *not* the number of emission angles for which data are acquired. Table 1 compares the main features of ARXPS to those of standard XPS depth profiling.

Finally, it should be noted that depth probed by XPS can be also varied using a tunable-energy excitation source, such as synchrotron radiation (SR), since the photoelectron escape depth depends on the photoelectron kinetic energy [37]. XPS spectra from different depths can be obtained by varying excitation energy. This technique can provide the depth profile nondestructively, just like the take-off angle variation technique. However, only a few studies have used this approach, probably due to the need for a large-scale installation to carry out the experiments and the mathematical problems involved in recovering the CDP; also, the fractional depth resolution that can be obtained is similar to that achieved with ARXPS measurements.

Secondary ion mass spectrometry (SIMS)

Secondary ion mass spectrometry is based upon sputtering a few atomic layers from the surface of the sample through "primary ion" bombardment. A primary ion impact triggers a cascade of atomic collisions that induce the emission of atoms and atomic clusters. Although most of the atoms and molecules removed from the sample by the interaction of the primary beam and the sample surface are neutral, some percentage of them are ionized. These "secondary ions" are characteristic of the composition of the analyzed area. If the primary beam is composed of positively charged ions, the resulting ionization favors the production of negative ions, and primary beams of negative ions favor the generation of positive ions. These ions are then accelerated, separated according to their mass, and analyzed by a mass spectrometer. Finally, an image containing quantitative information is obtained for a selected mass. In [8], Benninghoven et al. detail the basic concepts, instrumental aspects and applications of SIMS.

Conventional SIMS systems equipped with ion beam depth profiling can achieve nanometer resolution at large depths, together with a high level of detection and quantification (below 1 ppm) [38, 39]. Nevertheless, such nanometric depth resolution is only obtained when using primary ion energies in the sub-keV range [40]. However, the advantages of lowering the impact energy are compromised by not only significant surface roughening but also a decrease in sputtering yield (proportional to the number of emitted/detected particles). The depth resolution is limited for a high ion flux, since energetic interactions of the

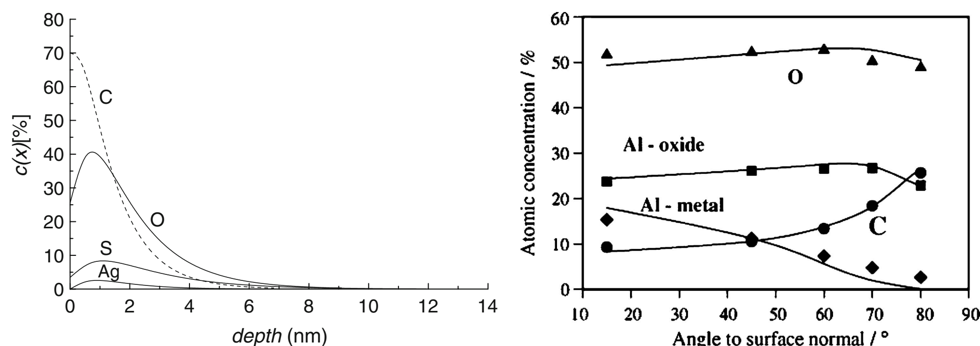

Fig. 4 *Left*: ARXPS depth profiles calculated using the experimental data collected for all species detected in an ultrathin layer of Ag deposited electrochemically on Pt using the general inversion algorithm described in [35]. *Right*: results of ARXPS investigations of a native Al oxide sample using a model of a C contamination/Al oxide/Al substrate multilayer. Taken from [36] and reproduced with the permission of Elsevier

Table 1 Comparison of the main features of the XPS and ARXPS configurations

	XPS + ion sputtering	ARXPS
Probing particle	Photons	Photons
Detected particle	Electrons	Electrons
Sputtering	Ion beam (noble gas) <10 keV	No
Atomic mixing?	Yes	No
Sampling depth (nm)	1–10	0.3–3
Depth resolution (nm)	1–2 nm (in the best cases) (with rotating samples)	~2–4 nm (in the worst cases)
Lateral resolution (μm)	~5	~5
Max. depth analysis (nm)	100–1000	10
Detection limit	0.01 atom%	0.01 atom%
Elemental range	All except H, He	All, except H, He
Reliable quantification (elemental composition)?	Yes but destroyed during sputtering	Yes
Destructive?	Yes	No
Chemistry information?	No, destroyed during sputtering	Yes
Vacuum (mbar)	10^{-10}	10^{-10}
Deconvolution needed?	Yes (difficult to determine the resolution function)	Yes (attenuation length function as resolution function)
Analysis time	Slow (hours)	Moderate (minutes)

primary ion with the sample lead to profile distortions due to the primary incorporation of the incident projectiles and the damage induced by the collision cascades. Different approaches are now being developed with the aim of achieving the ultimate depth resolution. Vandervorst recently reviewed these different approaches in order to assess if the SIMS method will be able to fulfil the needs of industrial semiconductor analysis [41].

A first approach (EXLE-SIMS) involves using extremely low bombardment energies as low as 100 eV. New primary ion columns called floating low-energy ion guns (FLIG) have been developed, as shown in Fig. 5, as a replacement for classical ion columns, in order to decrease the ion beam energy down to 100 eV while keeping chromatic aberrations at a low level in the newest generation of EXLE-SIMS techniques [42]. Several teams have already achieved a depth resolution of 1–1.2 nm by using primary ion energies of 100–550 eV [41, 43, 44]. This made it possible, for example, to better analyze interfaces in organic–inorganic multilayers (as shown in the left-hand panel in Fig. 6) for polymer solar cells [43]. Moreover, in [45], nanometer depth resolution was also obtained for a 50×(16 monolayers ^{28}Si/10 monolayers ^{30}Si) isotopic superlattice system (see the right-hand panel in Fig. 6) using a 1 keV Cs primary beam. The nature of the primary ions used has an important effect on the depth resolution. For example, the results obtained with cesium (Cs) ions are not as good as those achieved with oxygen (O) ions, which give a much larger decay length, even for

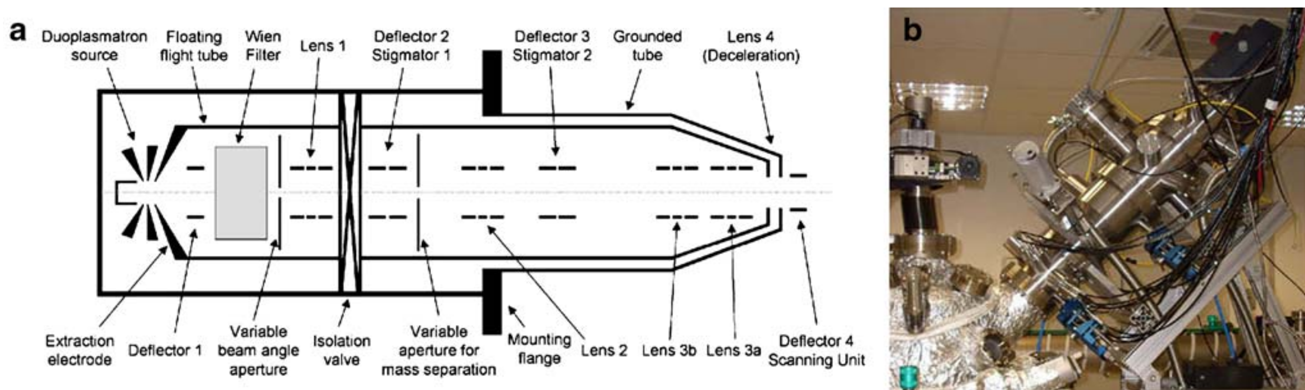

Fig. 5 Schematic drawing (*left*) and photograph (*right*) of the FLIG installed on the sputter deposition chamber of the prototype Storing Matter instrument. Taken from [42] and reproduced with the permission of Elsevier

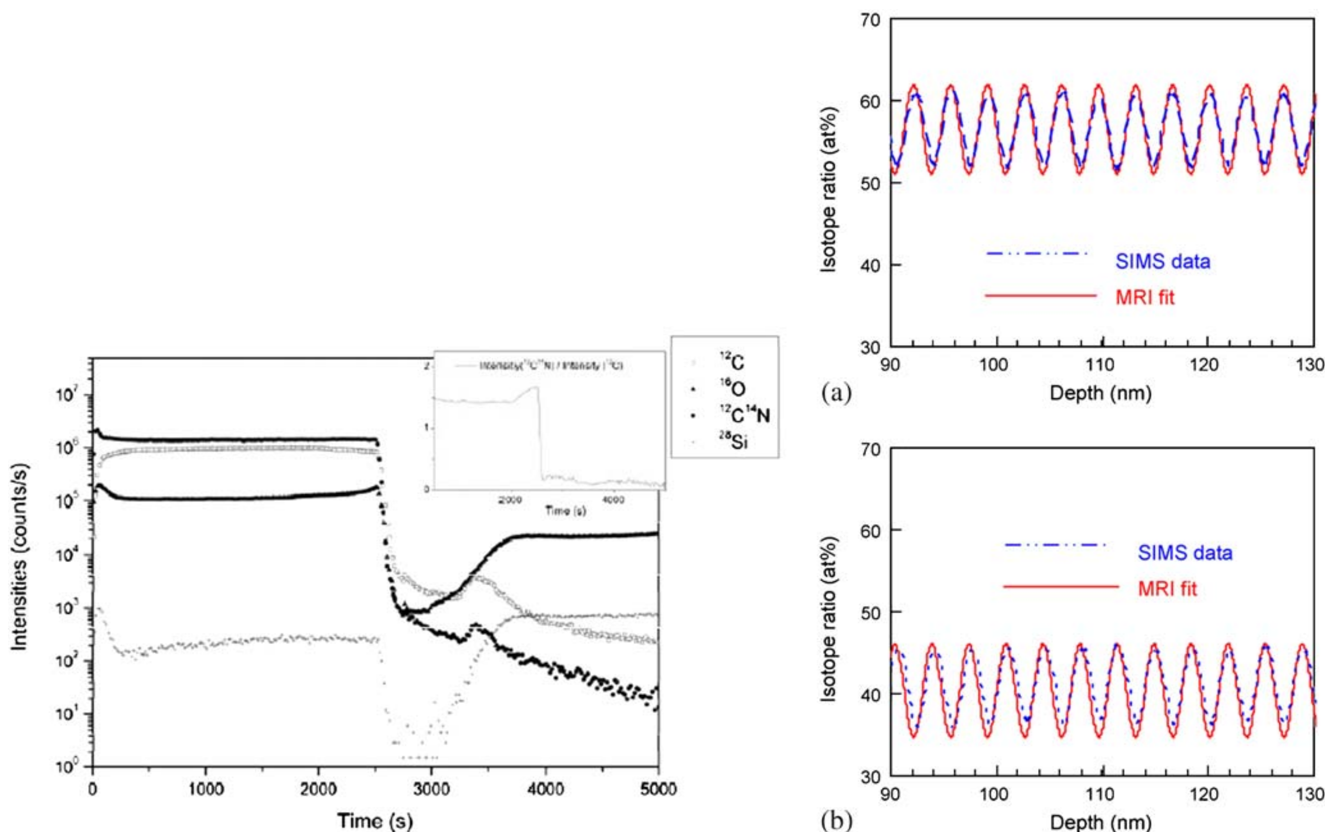

Fig. 6 *Left*: SIMS depth profiles obtained for a P3HT-P4VP:PCBM/PEDOT:PSS active layer with 17% PCBM (equivalent to C17) deposited on an oxidized silicon wafer, where ^{28}Si (*crosses*), ^{12}C (*squares*), ^{16}O (*triangles*) and ^{12}C^{14}N (*circles*) were probed. *Inset*: ^{12}C^{14}N signal normalized by the ^{12}C signal (polymer matrix) to attenuate possible matrix effects. The experiments reported here were carried out in ultrahigh vacuum (UHV) using a Cs^+ primary ion source with an impact energy of 500 eV and negative ion detection to optimize the secondary detection. The ^{12}C SIMS signal was used to identify the polymer layer, while the ^{12}C^{14}N SIMS signal was chosen to probe P4VP. Taken from [43] and reproduced with the permission of Wiley. *Right*: SIMS depth profiles of **a** ^{28}Si and **b** ^{30}Si isotopes in a 50×(16 monolayers ^{28}Si/10 monolayers ^{30}Si) superlattice system. The experiments were performed using a 1 keV Cs^+ ion beam at 45°. Taken from [45] and reproduced with the permission of Elsevier

energies as low as 150 eV [41]. The best depth resolution obtained for germanium (Ge) profiles in a thin (2.5 nm) SiGe layer grown in a Si substrate were achieved with a 100 eV O^+ primary ion beam and an impact angle of 57°. In theory, even lower primary ion energies will allow further decreases that will improve the depth resolution. Unfortunately, below 100 eV the sputtering efficiency (erosion rate) decreases quite rapidly, and both the time need to detect a sufficient number of ions and the time required for analysis rapidly increase. The detection limit also decreases as the primary ion energy is lowered. For example, in the case of boron detection in silicon, the detection limit worsens from 0.001 ppm at 10 keV to 0.1 ppm at 500 eV. Instrumental developments that enable improved primary beam currents in the 50–200 eV range are presently being targeted to improve the sputtering performance to the 1 nm/min level [41], but this is a huge challenge. In some cases, the use of oxygen (or some other elements with a low heat of sublimation) flooding at the same time as primary ion sputtering can increase the negative secondary ion yield, thus compensating for the lower speed of sputtering at low primary ion energies [46, 47]. Sample holder rotation can also be useful in conditions where high roughness is created in the bottom of the analysis crater, and especially when analysis at large depths (micrometer range) is needed. In such cases, rotating the sample holder decreases or suppresses roughening in the analyzed area, allowing for better depth resolution. Finally, it appears that the depth-resolution limits of EXLE-SIMS are close to being reached for the semiconductor industry, but for other applications—such as studies of the oxidation or the wear of thin films—this could become a very interesting tool for studying the first steps in degradation.

A second approach uses cluster beams instead of ions beams in order to improve the depth resolution. It was shown that the use of cluster beams (C60, Ir-based clusters) yields no advantage in terms of depth resolution, as the total energy appears to be more influential than the energy per constituent atom, and the reduction in the total energy is restricted by the onset of cluster deposition [48]. However, further exploration of these clusters may lead to more interesting results.

New approaches that aim to meet the higher depth-resolution targets, such as zero-energy SIMS or atom-probe tomography, eliminate the use of a primary ion beam. In the zero-energy SIMS concept the ion beam is completely absent [49, 50]. Localized material removal is instead based on the adsorption of reactive gases at the sample surface and the creation of a volatile compound. Selective material removal is achieved using an electron beam, which locally stimulates a chemical reaction between the adsorbed species and the matrix elements. Theoretically this process has monolayer depth resolution, as set by the monolayer adsorption and desorption processes, and a high spatial resolution (set by the spot size of the electron beam, which could be as small as a few nanometers), and it is quantitative, as the desorbed species are nonresonantly ionized using a laser beam. However, this method will tend to be applied to standard or very homogeneous samples, at least for the next few years, because many deficiencies can occur, such as preferential etching and/or outplating, nonplanar erosion, incomplete ionization, etc.

A second method that does not use a primary ion beam is atom-probe tomography [51–53]. Here, atom removal is induced by applying a very high (pulsed) electrical field. The emitted atoms are fully ionized (there is no matrix effect to consider during quantification) and detected in a spatially resolved time-of-flight detector. Due to the optical ion magnifications involved, spatial resolution is on the order of <0.5 nm. As the atoms are removed one by one, the depth resolution is on the same order as this. Clearly, the excellent three-dimensional resolution makes the method much more versatile than regular SIMS, in particular for the analysis of heterogeneous samples such as nanocomposite coatings. Complications and limitations arise from the need for special sample preparation (the formation of a needle-shaped specimen with a top radius of about 50 nm, which typically requires extensive focused ion beam milling), sample conductivity requirements that enable the propagation of the high-voltage pulse (this requirement is now partially relaxed due to the addition of laser-assisted erosion), the small field of view (<100 nm), which limits the total number of atoms analyzed and thus the achievable sensitivity ($>10^{18}$ at/cm^3), and the extensive (3D) data reconstruction needed. In practice, sample breakage (due to the large mechanical stresses induced by the strong electrical fields) is an important mechanism that limits the routine application of the atom probe. Finally, a very significant advantage of the atom probe relative to SIMS is its 3D resolution at the subnanometric scale, which enables heterogeneous samples and/or rough interfaces to be analyzed without any serious loss in depth resolution [54].

In conclusion, several approaches with improved depth resolution are being developed, with the most promising being zero-energy SIMS and atom-probe tomography, which target the sub-nm range, but these two approaches are much more complex to use than EXLE-SIMS. Table 2 presents a comparison between the figures of merit for ultralow-energy SIMS and those for a conventional system.

Glow-discharge optical emission spectroscopy (GDOES)

GDOES is a relatively new surface analysis technique with the advantages of moderate vacuum requirements and very high sputtering rates (typically >1 μm min^{-1}), which enable the CDP to be obtained in a few minutes with a depth resolution comparable to more standard techniques, such as AES, XPS or SIMS [4, 55–57]. During GDOES experiments, the samples are sputtered by Ar^+ ions and accelerated neutral species with very low energies (<50 eV). The sputtered atoms are then excited by the plasma and de-excited by emitting photons with a characteristic wavelength, enabling element discrimination. These photons are diffracted by a diffraction grating and collected by photomultiplier (PM) detectors positioned in a Rowland circle [10, 11]. Furthermore, the use of a radiofrequency (rf) source for sputtering extends the application of GDOES to the study of insulators used both as coatings and as substrates [58–60]. In the last few years, GDOES has been applied extensively to the study of multilayer depth profiling [17, 18, 61–65], although a serious loss of resolution with depth during GDOES analysis has been reported. The major factors contributing to this loss of resolution are related to the high erosion rate, sample heating, ion-induced surface roughening [66, 67], and in particular, the crater geometry during the sputtering process, which results in the mixing of the consecutive layers in a multilayer system when the individual layer thicknesses reach down to the nanometer scale [68–72].

Among the different strategies that are currently being employed to improve the depth resolution of GDOES depth profiling, we will focus here on: i) the use of pulsed sources; ii) the application of deconvolution algorithms and the modeling of multilayer profiles, and; iii) the utilization of plasma cleaning procedures prior to analysis.

The use of pulsed rf sources in GDOES analysis (pulsed glow discharge, or PGD) is based on the pioneering work of Winchester and Marcus [73]. Pulses of a short duration (10 μs to 1 ms) with various possible repetition rates (duty cycles) and high instantaneous powers (up to hundreds of watts) can therefore be generated. It has been reported in the literature [74–76] that such pulses produce an enhancement in the emission yield, resulting in increased sensitivity and lower detection limits together with simplified calibration curves due to the reduced self-absorption of the emission lines. Moreover, pulsed glow discharges cause a lower average power to be applied than in DC mode, and so they

Table 2 Comparison of the characteristics of SIMS and EXLE-SIMS

	SIMS	EXLE-SIMS
Probing particle	Ions	Ions
Detected particle	Ions (m/q)	Ions (m/q)
Sputtering	Ion beam <10 Kev	Ion beam <100 eV
Atom mixing?	Yes	Yes
Sampling depth (nm)	5	10
Depth resolution (nm)	5	1
Lateral resolution (nm)	100	100
Detection limit (ppm)	10^{-3}–10	10^{-1}–10
Elemental range	All	All
Calibration method	Complex (need standards)	Complex (need standards)
Destructive?	Yes	Yes
Isotope information?	Yes (+)	Yes (+)
Crater effect?	Yes (−)	Yes (−)
Crater diameter (mm)	<1	< 0.5
Vacuum (mbar)	10^{-10}	10^{-10}
Analysis time	Slow (hours)	Slow (hours)

are ideal for the analysis of heat-sensitive materials such as glasses, polymers and low-temperature metals. It is worth noting here the excellent review on pulsed glow discharges that was recently published by Belenguer and coauthors [77]. The application of pulsed GDOES to the depth-profiling analysis of materials has arisen due to the ability to control both the flatness of the crater and the sputtering rate using the pulsed source parameters (i.e., frequency and width). Therefore, thinner surface layers can be properly resolved using PGD, as shown in the initial works of Yang and Oxley [78, 79] for 10 nm Cu coatings on steel. More recently there have been published examples of the application of PGD to the analysis of lead zirconate titanate (PZT) thin films (which find significant use in microelectronic and microelectromechanical systems) [80] and thin-film solar cells based on Cu(In,Ga)Se_2 and Cu(In,Ga)S_2 multilayers [81].

As expressed above in Eq. 2, an experimentally obtained CDP is a convolution of the true depth profile and the response function of the experimental set-up. In the particular case of a GDOES depth profile, the response function is determined by the sputtering crater shape. The crater shape can change markedly when the interfaces between different materials are traversed in a multilayer depth profile. Therefore, mathematically describing the response function in GDOES analysis is not a trivial task. Oswald and coauthors [82] were the first to attempt to apply deconvolution procedures to GDOES depth profiles (although the method was initially designed for SIMS analysis). Based on this initial work, Präßler and coauthors [83] developed an iterative deconvolution algorithm where—using the calibrated mass–time profile, the partial densities of the sample constituents and the measured final shape of the sputtering crater as input data—the depth profiles are improved by utilizing information on crater formation. In Fig. 7 (left-hand panel), an example of the successful application of such a deconvolution procedure to a Cu/CrNi multilayer system is presented. Years later, in the excellent review by Winchester and Payling [10], it was written that this success “makes deconvolution a real and exciting possibility for GDOES.” Nevertheless, more than a decade later, deconvolution procedures are yet to be integrated into any commercially available GDOES software. In an alternative approach, Escobar and Albella [84] recently reported on a simple model for interpreting and predicting the depth profiles of periodic multilayer structures of two elements, where the individual layer thicknesses are in the range of 10–100 nm (i.e., within the order of magnitude of roughness induced when depth profiling using GDOES techniques). The model is based on the assumption that the surface roughening produced by the ion bombardment gives rise to the partial mixing of the layers and their interfaces, leading to a smoothing of the otherwise abrupt profiles. Fitting the model to the experimental profiles for a set of samples made of alternating Ti and Cr layers, with thicknesses varying over a wide range, allows the degradation constant *b* (pre-exponential factor) to be obtained for each material. The values resulting from the fitting procedure correlate with the erosion rates of Ti and Cr, and support the idea that the layer broadening of each material is determined by its erosion rate. The degree of adjustment can be considered to be quite acceptable (see the right-hand panel of Fig. 7) for most of the samples investigated, taking into account the approximations involved.

Fig. 7 *Left*: composition depth profile of 100 nm thick Cu/CrNi multilayers on Si: **a** after deconvolution with a constant crater shape (the result is very similar to the unconvoluted profile); **b** after deconvolution with iteration to determine the uneven crater shape. Taken from [83] and reproduced with the permission of Elsevier. *Right*: **a** the GDOES experimental depth profile of a 10×(70 nm Ti/150 nm Cr) multilayer; **b** the simulated depth profile obtained using the nominal individual thicknesses from (**a**) and the degradation constant shown in Table 1 of [84]. Reproduced with the permission of Elsevier

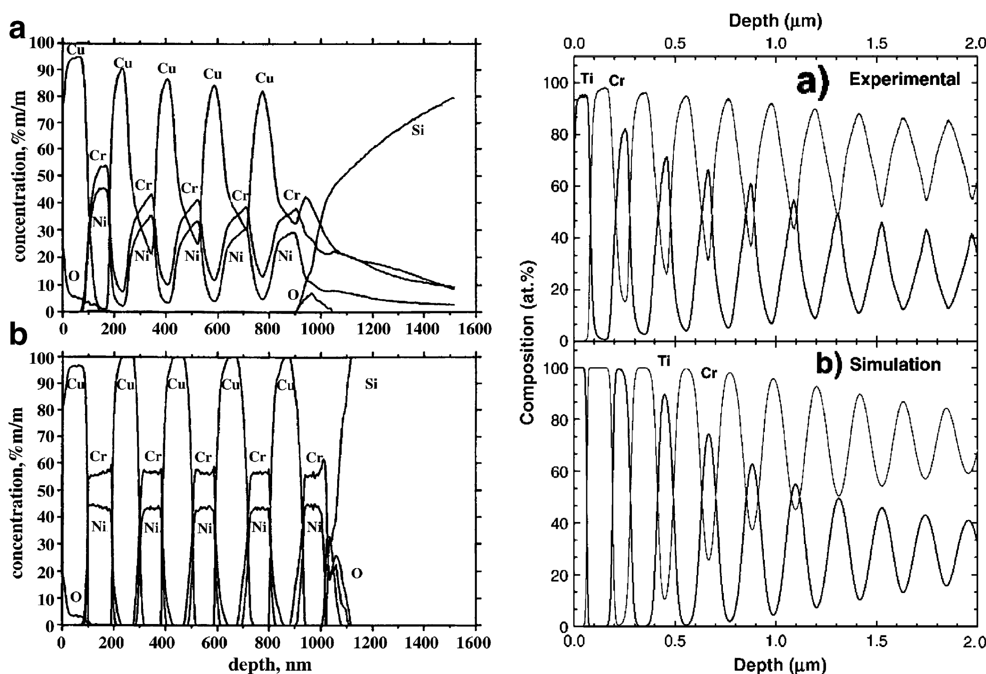

Finally, it is clear that in order to be able to analyze ultrathin layers near the surface using GDOES, rapid stabilization of the plasma at the start of the sputtering process is required. The technique where a sacrificial sample (typically a monocrystalline silicon wafer [85]) is employed to remove the contaminants (carbon, oxygen, hydrogen) from the inner walls of the anode prior to the analysis of the sample has been extensively applied by GDOES users. Molchan et al. have recently proposed [86] that this procedure can be improved by using a low-energy plasma (<5 W) to gently remove contaminant from the surface of the sample. In their work they demonstrate how such a treatment is below the sputtering threshold and does not cause any damage to the analyzed specimen. Figure 8 shows the large reduction in surface contaminants (tenfold for the carbon intensity) achieved when the plasma cleaning procedure is applied to an electropolished aluminum sample. Moreover, note how the total plasma response (*Fi*) stabilizes more rapidly. This plasma cleaning method has been implemented for routine surface analysis in the latest version of the QUANTUM software from Horiba Jobin Yvon instruments.

In conclusion, since GDOES is a relatively novel technique for ultrathin depth profiling, there is more room to improve its resolution. The use of soft plasma cleaning prior to sputtering using pulsed discharges, and the application of deconvolution procedures afterwards, will surely turn GDOES into an ideal technique for subnanometer depth profiling in terms of its ease of use and the accuracy of the results it yields. Table 3 compares the expected benefits of an optimized GDOES (OPT-GDOES) to the typical features of standard GDOES analysis.

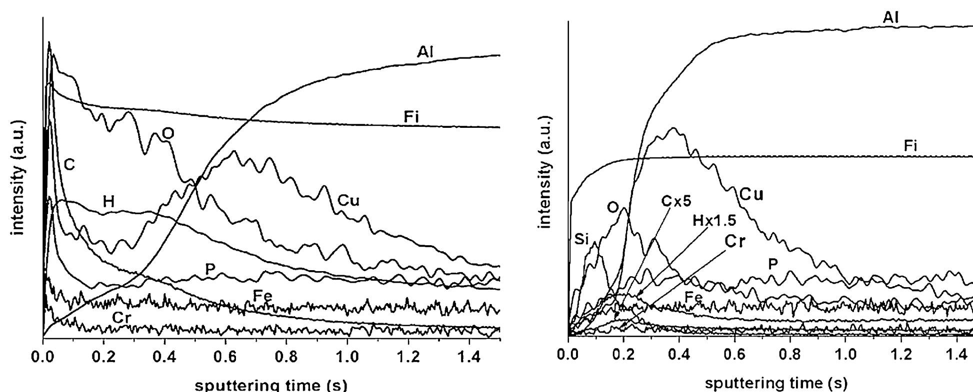

Fig. 8 GD OES depth profile of an electropolished aluminum sample, obtained at 750 Pa and 35 W, after no plasma cleaning (*left*) and after sputtering the silicon wafer for 1 min and then cleaning the specimen at 750 Pa and 3 W for 1 min (*right*). Note the reduction in contaminants (tenfold for carbon) in the right-hand depth profile. Taken from [86] and reproduced with the permission of Elsevier

Table 3 Comparison of the characteristics of standard GDOES with the expected figures of merit for an optimized GDOES (OPT-GDOES) method that utilizes soft plasma cleaning, pulsed source sputtering and deconvolution procedures

	GDOES	OPT-GDOES
Probing particle	Ions	Ions
Detected particle	Photons	Photons
Sputtering	DC/RF <50 eV	Pulsed RF
Atom mixing?	No	No
Max. depth analysis (μm)	>100	>100
Depth resolution (nm)	2 nm at surface, but degrades rapidly with depth	Monolayer resolution at the surface and no worse than 1 nm for the first 100 nm
Lateral resolution (nm)	10^6	10^6
Detection limit (ppm)	1	1
Elemental range	All	All
Calibration method	Complex (need standards)	Complex (need standards)
Destructive?	Yes	Yes
Isotope information?	Only deuterium	Only deuterium
Crater effect?	Yes	Strongly reduced by the pulsed source and deconvolution
Crater diameter (mm)	4	4
Vacuum (mbar)	10^{-2}	10^{-2}
Analysis time	Very fast (seconds)	Very fast (seconds)

Rutherford backscattering spectroscopy (RBS)

Analysis by Rutherford backscattering spectroscopy (RBS) is based on the detection of light, monoenergetic particles (normally alpha particles) scattered by the positively charged nuclei of heavier elements [12, 13]. This interaction can be described by classical scattering that takes into account the Coulomb potential, and so one of the benefits of RBS is that it provides quantitative analysis without the need for standards. A limitation of the technique is that the kinematics of the collision are insensitive to the electronic configuration of the scattering element, so information about the chemical bonding of the target is not attainable.

In RBS, the energy (E) of a backscattered projectile with an initial energy E_0 and a given mass m_1 is measured by the detector system. For a given scattering angle θ, and assuming that the collision takes place at the sample surface, the reduction in the projectile energy ($\Delta E = E_0 - E$) is a direct measure of the mass of the target element (m_2). Since the mass of the projectile is known, the corresponding energy can be obtained from the kinematic factor, as given by [12, 13]:

$$K = \frac{E}{E_0} = \left(\frac{m_1}{m_1 + m_2}\right)^2 \left(\cos\theta \pm \sqrt{\left(\frac{m_2}{m_1}\right)^2 - \sin^2\theta}\right)^2 \tag{4}$$

Equation 4 shows that heavier elements appear at higher energy channels in the RBS spectrum. Also, large scattering angles ($\theta \sim \pi$) are used to increase the mass resolution $[\sim(\partial K/\partial m_2)^{-1}]$.

The element sensitivity of RBS is also an important factor in accurate compositional analysis. This magnitude is proportional to the probability of scattering or the scattering cross-section $\sigma(\theta)$. For large-angle scattering ($\theta \sim \pi$), the differential scattering cross-section (the probability of scattering into a differential solid angle $d\Omega$) for the Coulomb potential can be simplified to

$$\frac{d\sigma(\theta)}{d\Omega} \xrightarrow{\theta \to \pi} \left(\frac{Z_1 Z_2 e^2}{4E}\right)^2 \frac{1}{\sin^4\theta} \tag{5}$$

where e represents the electron charge in cgs units ($e^2 \sim 1.44 \times 10^{-13}$ MeV cm), and Z_1 and Z_2 are the atomic numbers of the projectile and the target element, respectively. As derived from Eq. 5, the sensitivity of RBS increases with Z and decreases with E.

When the projectile penetrates into the solid, there are inelastic energy losses, as well as those that occur during the elastic scattering event. In the energy range for RBS (MeV), these losses are mainly due to electronic excitations of the target atoms [12, 13]. Energy losses occur during both inward and outward trajectories, and the total energy loss can be used to determine the thickness of the material traversed. This is the basis of RBS depth profiling. In this case, the energy loss per unit length [$S(E) = dE/dx$] of the projectile through the target must be

known, and, for the energies typical of RBS, this decreases monotonously with E [12]. Assuming that the energy loss is constant in the detection energy window, or that the energy loss is negligible (surface energy approximation), ΔE for a scattering event produced at a depth $x = d$ is given by:

$$\Delta E = Sd\left(\frac{K}{\sin\alpha} + \frac{1}{\sin\beta}\right) = d[S] \quad (6)$$

where K is the kinematic factor given in Eq. 4, and α and β are the incident and exit angles (with respect to the surface normal), respectively, for the projectile. $[S]$ denotes the energy loss factor or S factor.

The limit for the depth resolution (δx) of RBS can be derived from Eq. 6 as

$$\delta x = \frac{\delta \mathrm{E}}{[\mathrm{S}]} \quad (7)$$

From Eq. 7, it is clear that the factors that have the greatest influence on the depth resolution of RBS are the beam monochromaticity, the $[S]$ value, and the energy resolution of the detector system. In particular, for a given detector energy resolution, the depth sensitivity will be optimized by maximizing $[S]$. Of course, the sample characteristics (the elements to be detected, the roughness, the quality of the interfaces, etc.) will also have an impact on the achievable depth resolution. It should also be noted that the depth resolution will degrade dramatically with increasing depth due to straggling effects and the loss of beam monochromaticity.

Several approaches can be used to improve the depth resolution in the near-surface region. First, the energy loss factor $[S]$ given in Eq. 7 can be increased by using lower beam energies or by increasing α and/or β (projected range of the reduced ion). This is illustrated in Fig. 9, where 10 nm sequential layers of AlN and CrN are resolved by simultaneously decreasing and increasing the beam energy and α, respectively [18]. Another way to increase $[S]$ is to use heavier ions. However, this is not a good alternative unless mass-resolved detectors are used, since the energy resolution of the detectors will also deteriorate as the mass of the detected particle increases [12].

Standard RBS analysis employs solid-state silicon (Si) detectors. In this case, the energy of the detected particle is proportional to the height of the pulse generated by the detector. Therefore, except for the need for an accelerator facility, the instrumentation required for RBS is rather simple. The energy resolution of an Si detector is 15–25 keV, which gives a resolving power of $\delta E/E \sim 10^{-2}$. This provides a typical depth resolution of ~10 nm, which can be further improved to ~2 nm by using grazing incidence configurations [12]. However, when a grazing incidence configuration is used, the roughness of the sample will be a strong limiting factor.

An alternative way of further increasing the RBS depth resolution below the nm range ($\delta E/E < 10^{-3}$) is to use better detector systems. This can be achieved by using small magnetic spectrometers (MS) [87–90]. As an illustrative example of such instrumentation, a photograph of an MS is shown in the left-hand panel of Fig. 10. In these systems, the scattered beam travels through a magnetic field that deflects the ion trajectory to different positions in the focal plane. This allows the particle energy to be determined with high precision. In particular, a resolution of a few keV can be achieved (ten times lower than for Si detectors), thus providing high-resolution (HR) spectra and the capacity to resolve nanometer-layer stacks [91, 92]. Moreover, monolayer resolution by RBS has also been reported [93]. Table 4 presents a comparison between the main features of standard RBS and HR-RBS.

As an illustrative example of HR-RBS analysis, the right-hand panel of Fig. 10 shows a 30×(1.9 nm Mo/2.33 nm B_4C) multilayer structure and the corresponding

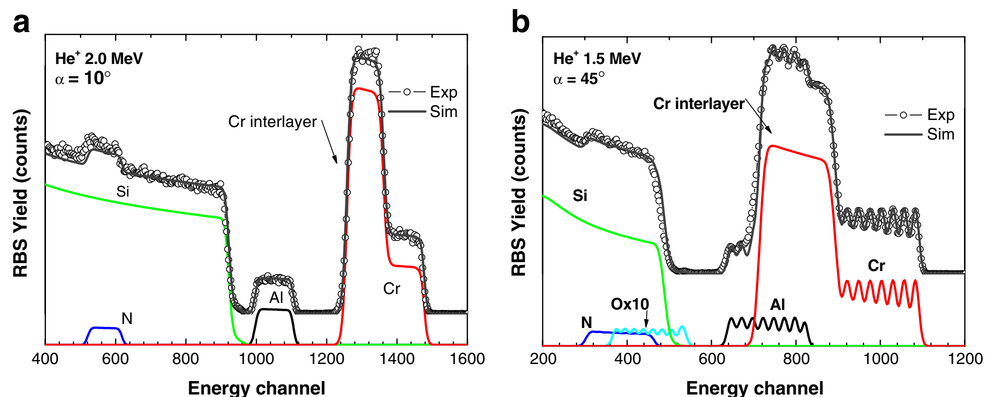

Fig. 9 RBS spectra for eight stacks of AlN/CrN bilayers with different measurement configurations. The thickness of each individual layer is 10 nm. The data clearly show how the individual layers can be resolved (**b**) by both reducing and increasing the beam energy and angle of incidence (α), respectively. Modified from [18] and reproduced with the permission of Elsevier

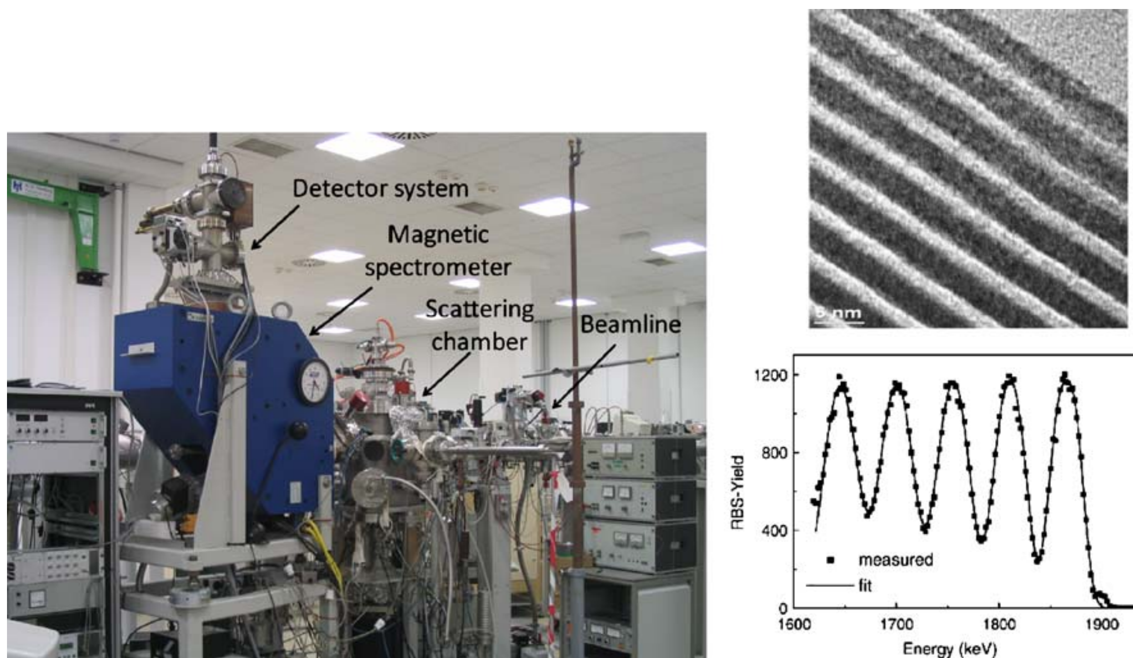

Fig. 10 *Left*: photograph of the Browne–Buechner MS at Forschungszentrum Dresden-Rossendorf (FZD) in Germany. The main components of the instrumentation are indicated by *arrows*. *Right*: a TEM image of a Mo/B_4C multilayer on Si is shown in the *top panel*. The *dark and bright stripes* correspond to the Mo and B_4C layers, respectively. The HR-RBS spectrum as measured with 2 MeV C^+ ions at an incidence angle of 17.5° and a scattering angle of 35.5° is presented in the *bottom panel*. Taken from [91] and reproduced with the permission of Elsevier

spectrum taken with an MS (from [91]). The experimental data clearly show fringes that correspond to the signals from individual Mo layers. The HR-RBS data can also be fitted, although the analysis is more complex than it is for conventional RBS measurements. Recently, HR-RBS in combination with channeling measurements were obtained using an MS for the study of ultrathin HfO_2/Si(001) [94, 95], Si(001)/HfSiON [96] and SiO_2/Si [97, 98] structures. The channeling configuration provides simultaneous structural and compositional information about the sample. In this case,

Table 4 Comparison of the main features of RBS and HR-RBS configurations

	RBS	HR-RBS
Probing particle	Light ions	Light ions
Detected particle	Backscattered ions/neutrals	Backscattered ions
Sputtering?	No	No
Atom mixing?	No	No
Sampling depth (nm)	From nm up to few microns	Limited to several tens of nm
Depth resolution (nm)	5–10 nm	<1 nm (only at the near-surface)
Lateral resolution (nm)	10^5	10^5
Detection limit	10^{-1}–10^{-2} at.% for heavy elements)	10^{-2}–10^{-3} at.% (for heavy elements)
Elemental range	All, except H, He	All, except H, He
Data analysis	Simple	Complex
Destructive?	No	No
Chemistry information?	No	No
Vacuum (mbar)	10^{-6}	10^{-6}
Analysis time	Moderate (minutes)	Moderate (minutes)
Energy resolution	15–20 keV	1 keV ($\Delta E/E \sim 10^{-3}$)
Instrumentation (detection system)	Simple (solid-state silicon detectors)	Complex (magnetic spectrometers)

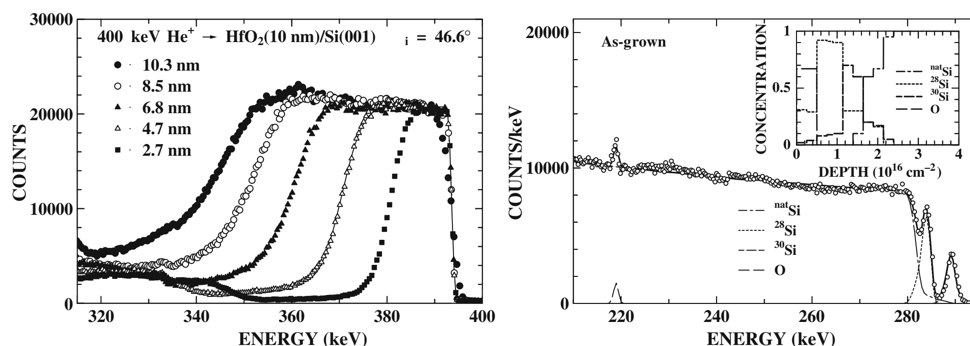

Fig. 11 *Left*: examples of HR-RBS spectra for HfO_2/Si(001) observed during grazing-angle sputtering by 1 keV Xe^+. The results obtained when the HfO_2 layer thickness was 10.3, 8.5, 6.7, 4.6 and 2.7 nm are shown. Taken from [95] and reproduced with the permission of Elsevier. *Right*: observed HRBS spectrum for an as-grown Si isotope heterostructure ($^{28}Si/^{30}Si/^{na}tSi$) sample. Elemental depth profiles determined through simulations of the HRBS spectra are shown in the *inset*. A native SiO_2 layer 0.7 nm in thickness and weak intermixing between the adjacent epitaxial layers can be observed. Taken from [98] and reproduced with the permission of Elsevier

the probe beam is aligned with a major direction of symmetry in the crystalline structure, which results in a greater reduction in backscattering as the quality of the crystal increases. Some relevant examples of such studies are shown in Fig. 11.

Final remarks: combining high-resolution techniques

Despite the important technical developments achieved in surface analysis techniques regarding depth resolution, it is clear that there is no unique method for completely characterizing subnanometer systems. It is only by using a suitable combination of high-resolution techniques that we can achieve a proper description of such complex systems in terms of composition, chemical states, quality of interfaces, etc. In this regard, Yamamoto et al. [99] conducted a combined low E-SIMS, HR-RBS and XPS analysis of ultrathin films of HfSiON (2.5 nm) for use as new gate dielectrics. They presented oxygen and nitrogen profiles of these thin films (see the left-hand panel of Fig. 12) and precisely quantified the nitrogen contents of the samples. Moreover, in an excellent, recently published study by Kimura et al. [100], HR-RBS and ARXPS were used to analyze two different gate stack structures, 2.5 nm HfO_2/1.6 nm SiON/Si(001) and 4 nm HfO_2/1 nm SiO_2/Si (001). As mentioned above, ARXPS is a very powerful tool for studying chemical states in ultrathin layers. However, complicated models with many degrees of freedom are needed to fit the ARXPS data. In this work, the authors cleverly applied composition depth profiles that had been accurately obtained by HR-RBS as constraints when determining chemical-state depth profiles for their samples (see the right-hand panel in Fig. 12). This study represents one of the best examples of what can be expected to be achieved in the coming years within the field of depth profiling ultrathin layers.

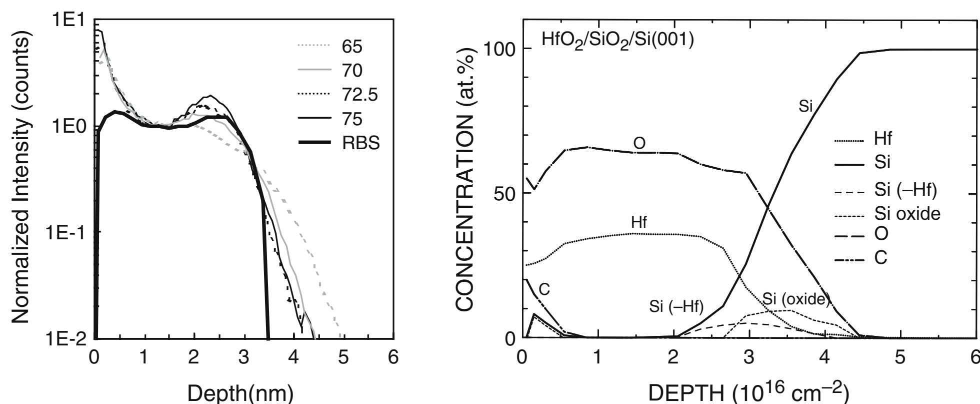

Fig. 12 *Left*: comparison of SIMS CsO^+ depth profiles of ultrathin 2.5 nm HfSiON films grown on 1 nm SiO_2/Si with an HR-RBS oxygen profile. The SIMS profiles were obtained using 500 eV Cs^+ and different impact angles from 65 to 75°. Taken from [99] and reproduced with the permission of Elsevier. Right: composition depth profiles of 4 nm HfO_2/1 nm SiO_2/Si, obtained via HRBS measurements (*thick lines*). The profiles of oxidized Si and Si–Hf bonds derived by combined ARXPS/HR-RBS analysis are also shown (*thin lines*). Taken from [100] and reproduced with the permission of Elsevier

Acknowledgments The authors wish to thank K. Kimura (Kyoto University), P. Chapon (Horiba Jobin Yvon), J. Wang (Max Planck Institute for Metals Research), V. Hofmmann (IFW Dresden) and R. Grötzschel (Forschungszentrum Dresden-Rossendorf) for their valuable comments during the preparation of the manuscript. This work was financially supported by the Spanish Ministry of Science and Innovation (projects MAT2008-06618-C02-01, FUNCOAT CSD2008-00023 and RyC2007-0026).

References

1. Werner HW, Garten RPH (1984) A comparative study of methods for thin-film and surface analysis. Rep Prog Phys 47:221–344
2. Alford TL, Feldman LC, Mayer JW (eds) (2007) Fundamentals of nanoscale film analysis. Springer, New York
3. Hofmann S (1990) In: Briggs D, Seah MP (eds) Practical surface analysis by Auger and X-ray photoelectron spectroscopy. Wiley, Chichester
4. Oswald S, Baunack S (2003) Comparison of depth profiling techniques using ion sputtering from the practical point of view. Thin Solid Films 425:9–19
5. Hofmann S (1991) Compositional depth profiling by sputtering. Prog Surf Sci 36(1):35–87
6. Oswald S, Reiche R (2001) Binding state information from XPS depth profiling: capabilities and limits. Appl Surf Sci 179(1-4):307–315
7. Reniers F, Tewell C (2005) New improvements in energy and spatial (*x*, *y*, *z*) resolution in AES and XPS applications. J Electron Spectrosc Relat Phenom 142:1–25
8. Benninghoven A, Rüdenauer FG, Werner HW (eds) (1987) Secondary ion mass spectrometry: basic concepts, instrumental aspects, applications, and trends. Wiley, New York, p 1227, ISBN 0471519456
9. Chatzitheodoridis E, Kiriakidis G, Lyon I (2002) Secondary ion mass spectrometry and its application to thin film characterization. In: Nalwa HS (ed) Handbook of thin film materials—processing, characterisation and properties. Academic, New York, pp 637–683
10. Winchester MR, Payling R (2004) Radio-frequency glow discharge spectrometry: a critical review. Spectrochim Acta Part B 59:607–666
11. Bings NH, Bogaerts A, Broekaert JAC (2008) Atomic spectroscopy. Anal Chem 80(12):4317–4347
12. Chu WK, Mayer JW, Nicholet MA (1978) Backscattering spectrometry. Academic, New York
13. Tesmer JR, Nastasi M (2005) Handbook of modern ion beam material analysis. MRS, Pittsburgh
14. Bardi U, Chenakin SP, Ghezzi F, Giolli C, Goruppa A, Lavacchi A, Miorin E, Pagura C, Tolstogouzov A (2005) High-temperature oxidation of CrN/AlN multilayer coatings. Appl Surf Sci 252(5):1339–1349
15. Aouadi SM, Schultze DM, Rohde SL, Wong K-C, Mitchell KAR (2001) Growth and characterization of Cr_2N/CrN multilayer coatings. Surf Coat Technol 140(3):269–277
16. Miyagawa S, Baba K, Nakao S, Ikeyama M, Saitoh K, Miyagawa Y (1998) Effects of ion beam mixing on the depth profiles of thin metal layer in TiO_2. Nucl Instrum Meth B 141(1-4):467–471
17. Thobor A, Rousselot C, Mikhailov S (2003) Depth profiles study of n(TiN+AlN) bilayers systems by GDOES and RBS techniques. Surf Coat Technol 174–175:351–359
18. Escobar Galindo R, Forniés E, Gago R, Albella JM (2006) Nanometric resolution in glow discharge optical emission spectroscopy and Rutherford backscattering spectrometry depth profiling of metal (Cr, Al) nitride multilayers. Spectrochim Acta Part B 61 (5):545–553
19. Perez-Mariano J, Caro J, Colominas C (2006) TiN/SiNx submicronic multilayer coatings obtained by chemical vapor deposition in a fluidized bed reactor at atmospheric pressure (AP/FBR-CVD). Surf Coat Technol 201:4021–4025
20. Shimizu K, Brown GM, Habazaki H, Kobayashi K, Skeldon P, Thompson GE, Wood GC (1999) Impurity distributions in barrier anodic films on aluminium: a GDOES depth profiling study. Electrochim Acta 44:2297–2306
21. Oladeji IO, Chow L (2005) Synthesis and processing of CdS/ZnS multilayer films for solar cell application. Thin Solid Films 474(1-2):77–83
22. McIntyre NS, Johnston D, Chauvin WJ, Lau WM, Nietering K, Schuetzle D, Shankar K, Macdonald JE (1985) SIMS depth profiling of multilayer metal-oxide thin films—improved accuracy using a xenon primary ion. Nucl Instrum Meth B 12 (3):389–395
23. Lee HY, Jung WS, Han JG, Seo SM, Kim JH, Bae YH (2005) The synthesis of CrSiN film deposited using magnetron sputtering system. Surf Coat Technol 200(1-4):1026–1030
24. Albers T, Neumann M, Lipinsky D, Benninghoven A (1993) XPS and SIMS/SNMS measurements on thin metal oxide layers. Appl Surf Sci 70–71(1):49–52
25. Rincón C, Zambrano G, Carvajal A, Prieto P, Galindo H, Martínez E, Lousa A, Esteve J (2001) Tungsten carbide/diamond-like carbon multilayer coatings on steel for tribological applications. Surf Coat Technol 148:277
26. Bubert H, Grallath E, Quentmeier A, Wielunski M, Borucki L (1995) Comparative investigation on copper oxides by depth profiling using XPS, RBS and GDOES. Fresenius J Anal Chem 353:456–463
27. Escobar Galindo R, Gago R, Lousa A, Albella JM (2009) Comparative depth profiling analysis of nanometre metal multilayers by ion probing techniques. Trends Anal Chem 28(4):494–505
28. Wang L, Nie X, Lukitsch MJ, Jiang JC, Cheng YT (2006) Effect of tribological media on tribological properties of multilayer Cr (N)/C(DLC) coatings. Surf Coat Technol 201:4341–4347
29. Wang JY, Starke U, Mittemeijer EJ (2009) Evaluation of the depth resolutions of Auger electron spectroscopic, X-ray photoelectron spectroscopic and time-of-flight secondary-ion mass spectrometric sputter depth profiling techniques. Thin Solid Films 517:3402–3407
30. Sanz JM, Palacio CY, Martínez Duart JM (1985) Análisis químico de películas delgadas mediante espectroscopías de superficie y sputtering. Afinidad 42:363
31. Hofmann S (2000) Ultimate depth resolution and profile reconstruction in sputter profiling with AES and SIMS. Surf Interface Anal 30:228–236
32. Cumpson PJ (1995) Angle-resolved XPS and AES: depth-resolution limits and a general comparison of properties of depth-profile reconstruction methods. J Electron Spectrosc Relat Phenom 73:25–52
33. Palacio C, Martínez Duart JM (1983) Deconvolution methods applied to sputter depth profiles at interfaces. Thin Solid Films 105:25–32
34. Palacio C, Martínez Duart JM (1985) Correction of the escape depth effect in sputter depth profiles. Thin Solid Films 129:49–51
35. Palacio C, Ocón P, Herrasti P, Díaz D, Arranz A (2003) XPS and ARXPS study of silver underpotential deposition on platinum in acid solution. J Electroanal Chem 545:53
36. Oswald S, Reiche R, Zier M, Baunack S, Wetzig K (2005) Depth profile and interface analysis in the nm range. Appl Surf Sci 252:3–10

37. Yamamoto H, Yamada Y, Sasase M, Esaka F (2008) Non-destructive depth profile analysis for surface and buried interface of Ge thin film on Si substrate by high-energy synchrotron radiation X-ray photoelectron spectroscopy. J Phys Conf Ser 100:012044
38. Rincón C, Zambrano G, Carvajal A, Prieto P, Galindo H, Martínez E, Lousa A, Esteve J (2001) Tungsten carbide/diamond-like carbon multilayer coatings on steel for tribological applications. Surf Coat Technol 148:277
39. Lousa A, Romero J, Martínez E, Esteve J, Montala F, Carreras L (2001) Multilayered chromium/chromium nitride coatings for use in pressure die-casting. Surf Coat Technol 146–147:268–273
40. Hongo C, Tomita M, Takenaka M, Murakoshi A (2003) Accurate SIMS depth profiling for ultra-shallow implants using backside SIMS. Appl Surf Sci 203–204:264
41. Vandervorst W (2008) Semiconductor profiling with sub-nm resolution: challenges and solutions. Appl Surf Sci 255:805–812
42. Wirtz T, Mansilla C, Barrahma R, Verdeil C (2009) Novel floating low-energy ion gun for the storing matter instrument. Nucl Instrum Meth B 267:2583–2585
43. Sary N, Richard F, Brochon C, Leclerc N, Lévêque P, Audinot J-N, Berson S, Heiser T, Hadziioannou G, Mezzenga R (2009) A new supramolecular route for use of rod-coil block copolymers in photovoltaic applications. Adv Mater (accepted)
44. Guillot J, Valle N, Migeon H-N (2009) Mg profiling in 5 nm oxide layers by EXLE–SIMS. In: ECASIA 2009, 18–23 Oct 2009, Antalya, Turkey
45. Takano A, Shimizu Y, Itoh KM (2008) Film thickness determining method of the silicon isotope superlattices by SIMS. Appl Surf Sci 255:1430–1432
46. Kudriatsev Y, Villegas A, Gallardo S, Ramirez G, Asomoza R, Mishurnuy V (2008) Cesium ion sputtering with oxygen flooding: experimental SIMS study of work function change. Appl Surf Sci 254:4961–4964
47. Vandervorst W, Janssens T, Huyghebaert C, Berghmans B (2008) The fate of the (reactive) primary ion: sputtering and desorption. Appl Surf Sci 255:1206–1214
48. Krantzman KD, Kingsbury DB, Garrison BJ (2007) Cluster induced chemistry at solid surfaces: molecular dynamics simulations of keV C60 bombardment of Si. Nucl Instrum Meth B 255:238–241
49. Vanhove N, Lievens P, Vandervorst W (2008) Towards quantitative depth profiling with high spatial and high depth resolution. Appl Surf Sci 255:1360–1363
50. Vandervorst W (2003) US Patent 20030127591 (10 July 2003)
51. Thompson K, Larson DJ, Ulfig RM, Bunton JH, Kelly TF (2006) Analyzing Si-based structures in 3D with a laser-pulsed local electrode atom probe. Solid State Technol 49(6):65
52. Blavette D, Pareige C, Cadel E, Auger P, Deconihout B (2005) A journey in the atomic-scale microstructure of materials using atom-probe tomography. Chin J Phys 43(1):132–145
53. Deconihout B, Vurpillot F, Gault B, Da Costa G, Bouet M, Bostel A, Blavette D, Hideur A, Martel G, Brunei M (2007) Toward a laser assisted wide-angle tomographic atom-probe. Surf Interface Anal 39(2–3):278–282
54. Kelly TF, Miller MK (2007) Atom probe tomography. Rev Sci Instrum 78(3):31101(1–20)
55. Teo WB, Hirokawa K (1989) Depth analysis of metal coatings by glow discharge spectrometry with an argon helium gas mixture. Surf Interface Anal 14:143–152
56. Weiss Z (1990) Depth analysis of nickel thin films on silicon by glow discharge spectroscopy: the interface region. Surf Interface Anal 15:775–780
57. Weiss Z (1992) Quantitative-evaluation of depth profiles analyzed by glow discharge optical emission spectroscopy: analysis of diffusion processes. Spectrochim Acta Part B 47:859–876
58. Präßler F, Hoffmann V, Schumann J, Wetzig K (1995) Comparison of depth resolution for direct current and radiofrequency modes in glow discharge optical emission spectrometry. J Anal At Spectrom 10:677–680
59. Hodoroaba V, Unger WES, Jenett H, Hoffmann V, Hagenhoff B, Kayser S, Wetzig K (2001) Depth profiling of electrically non-conductive layered samples by RF-GDOES and HFM plasma SNMS. Appl Surf Sci 179:30–38
60. Payling R, Michler J, Aeberhard M (2002) Quantitative analysis of conductive coatings by radiofrequency-powered glow discharge optical emission spectrometry: hydrogen, d.c. bias voltage and density corrections. Surf Interface Anal 33(6):472–477
61. Beck U, Reiners G, Wirth Th, Hoffmann V, Präßler F (1996) Multilayer reference coatings for depth profile standards. Thin Solid Films 290–291:57–62
62. Shimizu K, Habazaki H, Skeldon P, Thompson GE (2003) Impact of RF-GDOES in practical surface analysis. Spectrochim Acta Part B 58:1573–1583
63. Shimizu K, Habazaki H, Skeldon P, Thompson GE (2003) Radiofrequency GDOES: a powerful technique for depth profiling analysis of thin films. Surf Interface Anal 35:564–574
64. Shimizu K, Habazaki H, Skeldon P, Thompson GE, Marcus RK (2001) Influence of interfacial depth on depth resolution during GDOES depth profiling analysis of thin alumina films. Surf Interface Anal 31:869–873
65. Pisonero J, Fernández B, Pereiro R, Bordel N, Sanz-Medel A (2006) Glow discharge spectrometry for direct analysis of thin and ultra-thin solid films. Trends Anal Chem 25:11–18
66. Shimizu K, Brown GM, Habazaki H, Kobayashi K, Skeldon P, Thompson GE, Wood GC (1999) Glow discharge optical emission spectrometry (GDOES) depth profiling analysis of anodic alumina films: a depth resolution study. Surf Interface Anal 27:24–28
67. Shimizu K, Brown GM, Habazaki H, Kobayashi K, Skeldon P, Thompson GE, Wood GC (1999) Impurity distributions in barrier anodic films on aluminium: a GDOES depth profiling study. Electrochim Acta 44:2297–2306
68. Hoffmann V, Dorka R, Wilken L, Hodoroaba VD, Wetzig K (2003) Present possibilities of thin-layer analysis by GDOES. Surf Interface Anal 35(7):575–582
69. Quentmeier A (1997) Sections 7.1 and 7.2. In: Payling R, Jones DG, Bengston A (eds) Glow discharge optical emission spectroscopy. Wiley, New York
70. Angeli J, Bengston A, Bogaerts A, Hoffmann V, Hodoroaba V, Steers E (2003) Glow discharge optical emission spectrometry: moving towards reliable thin film analysis: a short review. J Anal At Spectrom 18:670–679
71. Escobar Galindo R, Forniés E, Albella JM (2005) Interfacial effects during the analysis of multilayer metal coatings by radio-frequency glow discharge optical emission spectroscopy: Part 1. Crater shape and sputtering rate effects. J Anal At Spectrom 20:1108–1115
72. Escobar Galindo R, Forniés E, Albella JM (2005) Interfacial effects during the analysis of multilayer metal coatings by radio-frequency glow discharge optical emission spectroscopy: Part 2. Evaluation of depth resolution function and application to thin multilayer coatings. J Anal At Spectrom 20:1116–1120
73. Winchester MR, Marcus RK (1992) Emission characteristics of a pulsed, radio-frequency glow discharge atomic emission device. Anal Chem 64(18):2067–2074
74. Payling R, Michler J, Aeberhard M, Popov Y (2003) New aspects of quantification in r.f. GDOES. Surf Interface Anal 35(7):583–589
75. Nelis TH, Aeberhard M, Hohl M, Rohr L, Michler J (2006) Characterisation of a pulsed rf-glow discharge in view of its use in OES. J Anal At Spectrom 21(2):112–125
76. Hoffmann V, Efimova VV, Voronov MV, Smíd P, Steers EBM, Eckert J (2008) Measurement of voltage and current in continuous

and pulsed rf and dc glow discharges. J Phys Conf Series 133:012017
77. Belenguer PH, Ganciu M, Guillot PH, Nelis TH (2009) Pulsed glow discharges for analytical applications. Spectrochim Acta B 64(7):623–641
78. Yang C, Ingeneri K, Mohill M, Harrison WW (1999) Depth profiling of thin films with pulsed glow discharge atomic emission spectrometry. Anal Chem 71(23):5328–5334
79. Oxley E, Yang C, Harrison WW (2000) Quantitative depth analysis using microsecond pulsed glow discharge atomic emission spectrometry. J Anal At Spectrom 15(9):1241–1246
80. Schwaller P, Aeberhard M, Nelis T, Fischer A, Thapliyal R, Michler J (2006) Rapid depth profiling of lead zirconate titanate (PZT) thin films by pulsed glow-discharge optical emission spectroscopy. Surf Interface Anal 38:757–760
81. Efimova V, Hoffmann V, Eckert J, Abou-Ras D, Dietrich J (2009) Pulsed glow discharge: from electrical parameters to application in GDOES. In: Colloquium Spectroscopicum Int XXXVI, 30 Aug—3 Sept 2009, Budapest, Hungary
82. Oswald S, Hoffmann V, Ehrlich G (1994) Contributions to computer-aided interpretation of ion sputtering depth profiling. Spectrochim Acta Part B 49:1123–1145
83. Präßler F, Hoffmann V, Schumann J, Wetzig K (1996) Quantitative depth profiling in glow discharge spectroscopies: a new deconvolution technique to separate effects of an uneven erosion crater shape. Fresenius J Anal Chem 355:840–846
84. Escobar Galindo R, Albella JM (2008) Modelling of glow discharge optical emission spectroscopy depth profiles of metal (Cr,Ti) multilayer coatings. Spectrochim Acta Part B 63(3):422–430
85. Klemm D, Stangl M, Peeva A, Hoffmann V, Wetziga K, Eckert J (2008) Analysis of interface impurities in electroplated Cu layers by using GD-OES and TOF-SIMS. Surf Interface Anal 40:418–422
86. Molchan IS, Thompson GE, Skeldon P, Trigoulet N, Chapon P, Tempez A, Malherbe J, Lobo Revilla L, Bordel N, Belenguer Ph, Nelis T, Zahri A, Therese L, Guillot Ph, Ganciu M, Michleri J, Hohl M (2009) The concept of plasma cleaning in glow discharge spectrometry. J Anal At Spectrom 24:734–741
87. Grötzschel R, Klein Ch, Kruse O (2001) The Rossendorf broad-range magnetic spectrometer for high resolution RBS and NRA. Nucl Instrum Meth B 183:3–9
88. Kimura K, Joumori S, Oota Y, Nakajima K, Suzuki M (2004) High-resolution RBS: a powerful tool for atomic level characterization. Nucl Instrum Meth B 219–220:351–357
89. Arnoldbik WM, Wolfswinkel W, Inia DK, Verleun VCG, Lobner S, Reinders JA, Labohm F, Boerma DO (1996) A high resolution magnetic spectrograph for ion beam analysis. Nucl Instrum Meth B 118:566–572
90. Andrzejewski R, Lucas J, Guirao A, Gordillo N, Boerma DO (2006) A wide-angle magnetic spectrograph of a novel design. Nucl Instrum Meth B 249:939–942
91. Grötzschel R, Klein C, Mäder M (2004) RBS with high depth resolution using small magnetic spectrometers. Nucl Instrum Meth B 219–220:344–350
92. Nagel R, Alof C, Balogh AG, Arnoldbik WM, Boerma DO (2001) Study of magnetic multilayers by RBS with nanometer resolution. Nucl Instrum Meth B 183:140–145
93. Kimura K, Mannami M (1996) RBS with monolayer resolution. Nucl Instrum Meth B 113:270–274
94. Nakajima K, Joumori S, Suzuki M, Kimura K, Osipowicz T, Tok KL, Zheng JZ, See A, Zhang BC (2003) Strain profiling of HfO_2/Si(001) interface with high-resolution Rutherford backscattering spectroscopy. Appl Phys Lett 83:296
95. Sakai W, Nakajima K, Suzuki M, Kimura K, Brijs B (2006) Observation of the interfacial layer in HfO_2 (10 nm)/Si by high-resolution RBS in combination with grazing angle sputtering. Nucl Instrum Meth B 249:238–241
96. Suzuki M, Takashima A, Koyama M, Iijima R, Ino T, Takenaka M (2004) Characterization of Si(1 0 0)/HfSiON interface. Nucl Instrum Meth B 219–220:851–855
97. Nakajima K, Suzuki M, Kimura K, Yamamoto M, Teramoto A, Ohmi T, Hattori T (2006) Lattice distortion at SiO_2/Si(001) interface studied with high-resolution Rutherford backscattering spectroscopy/channeling. Jpn J Appl Phys 45:2467
98. Hosoi S, Nakajima K, Suzuki M, Kimura K, Shimizu Y, Fukatsu S, Itoh KM, Uematsu M, Kageshima H, Shiraishi K (2006) Observation of Si emission during thermal oxidation of Si(0 0 1) with high-resolution RBS. Nucl Instrum Meth 249:390–393
99. Yamamoto T, Miyamoto T, Karen A (2004) Quantification of nitrogen profiles in HfSiON films for gate dielectrics. Appl Surf Sci 231–232:561–564
100. Kimura K, Nakajima K, Zha M, Nohira H, Hattori T, Kobata M, Ikenaga E, Jin Kim J, Kobayashi K, Conarde T, Vandervorst W (2008) Combination of high-resolution RBS and angle-resolved XPS: accurate depth profiling of chemical states. Surf Interface Anal 40(3-4):423–426